Laghridat *et al.*
Protection and Control of Modern Power Systems (2022) 7:7
https://doi.org/10.1186/s41601-022-00227-0

Protection and Control of Modern Power Systems

ORIGINAL RESEARCH Open Access

Coordinated control by ADRC strategy for a wind farm based on SCIG considering low voltage ride-through capability

Hammadi Laghridat[1*], Ahmed Essadki[1] and Tamou Nasser[2]

Abstract

Wind farms are integrated with the power grid system to provide active and reactive power. Because in a wind farm, wind turbines (WTs) are highly coupled to their operating conditions, a central wind farm supervisory unit must take into account these conditions when producing power control references for each WT. The aim of this paper is to manage and control the active and reactive power of wind farms based on squirrel cage induction generators and back-to-back converters. The proportional distribution algorithm is used for distributing wind farm power to individual WTs. In addition, we consider the development of a local power management and control units for WTs. This is in order to extract the maximum available power from the wind, and to provide the active and reactive power predetermined by the transmission system operator, or to satisfy the grid code requirements considering Low Voltage Ride-through capability. The power dispatch strategy is to be used on all WTs using the distribution algorithm while ensuring the control loops using the proposed Active Disturbance Rejection Control strategy. The results demonstrate that the proposed strategies are efficient and can guarantee the safe integration of wind farms into the grid while respecting grid code requirements and power system stability.

Keywords: Wind farm, Wind generator, SCIG, ADRC, Supervision, Control

1 Introduction

Faced with the ever-increasing demand for electricity, and the need for reducing the use of polluting fossil fuels (oil, gas etc.), many countries have begun the shift to renewable energy sources (RESs) such as solar, wind, hydro, geothermal and biomass energy, etc. The real challenge is now taken seriously, both in terms of the policy of reducing greenhouse gas emissions by 2050 [1], and exploitation of renewable energy resources. In addition, in recent years, the environmental and economic benefits of RESs have increased, and RESs become the main solutions for addressing the greenhouse gas and pollution problems. Wind energy is one of the most promising and fastest growing RESs according to Wind-Europe's Central Scenario (WECS). By 2030, in the high scenario, it is expected that 397 GW of wind energy capacity will be installed in Europe, with 298.5 GW onshore and 99 GW offshore. Even in the low scenario, there will be 256.4 GW of wind capacity, with 207 GW onshore and 49 GW offshore. Wind power capacity will be equivalent to 20–35% of Europe's power demand (low and high scenarios) [2, 3]. According to the same report, Denmark had the highest proportion of wind power in its electricity demand last year (48%), followed by Ireland (33%) and Portugal (27%) [4].

Wind turbines (WTs) capture wind energy to provide mechanical power which is transformed to electrical power through electric generators. The recent development of power electronics systems has reflected positively on the WT technology, and as a result, variable speed wind energy conversion systems have rapidly

*Correspondence: hammadi.laghridat@um5s.net.ma
[1] Higher National School of Arts and Crafts (ENSAM), Mohammed V University, Rabat, Morocco
Full list of author information is available at the end of the article

developed. Therefore, WTs will operate with variable speed, which has the advantages of being able to capture the maximum energy over a wide range of wind speed, and improving the quality of the power produced by the WT. Commonly, the overall variable-speed WT technologies are divided into the doubly fed induction generator (DFIG)-based WT, squirrel cage induction generator (SCIG)-based WT and permanent magnet synchronous generator (PMSG)-based WT. A DFIG is directly connected to the grid via the stator side and indirectly via the rotor side using back-to-back converters, whereas SCIG and PMSG are connected to the utility grid using back-to-back power converters. SCIG-based and DFIG-based wind farms (WFs) have prominent advantages such as higher output power and electromechanical efficiency, improved power quality, higher power capture, wide range of speed variation, reduced turbine mechanical stress, and decoupled power control. However, DFIG-based WTs are more sensitive to voltage dips and grid disturbances because of their direct grid connection via the stator, and consequently, their dynamic performance becomes more complicated and poses many challenges to the grid [5].

Recently, several strategies have been investigated to improve WTs' fault ride-through (FRT) capability. These techniques can be divided into two types, hardware and software as illustrated in Fig. 1. Hardware strategies generally can be classified into two major categories. The first is based on reactive power injection methods, and [6] presents a review of different strategies for reactive power management of wind farms. The second category is based on a protection circuit and storage system [7, 8] present detailed reviews of the state of the art of protection circuits for WTs and key challenges for the storage system. Likewise, the software strategies can also be classified into two major categories, with the first based on traditional control strategies such as modified vector, hysteresis, feed forward transient current (FFTCC) and blade pitch angle control, and the second based on advanced nonlinear controllers such as sliding mode (SMC), backstepping (BSC), Fuzzy logic (FLC), model predictive (MPC), and active disturbance rejection control (ADRC). These control strategies used for WT FRT capability improvement are summarized in Fig. 1.

The majority of real systems are not only non-linear and varying in time, but also uncertain because of variations in the parameters described in their mathematical models. ADRC is developed to address the limitations of the traditional PID approach. This controller allows a very good elimination of the disturbances in real time. These disturbances can be numerous in WTs, given the complexity and the number of sensors involved. They also enable meeting the robustness requirements for the variations of the system parameters and the uncertainties of its mathematical model. At present, ADRC has been widely used in different areas, including wind

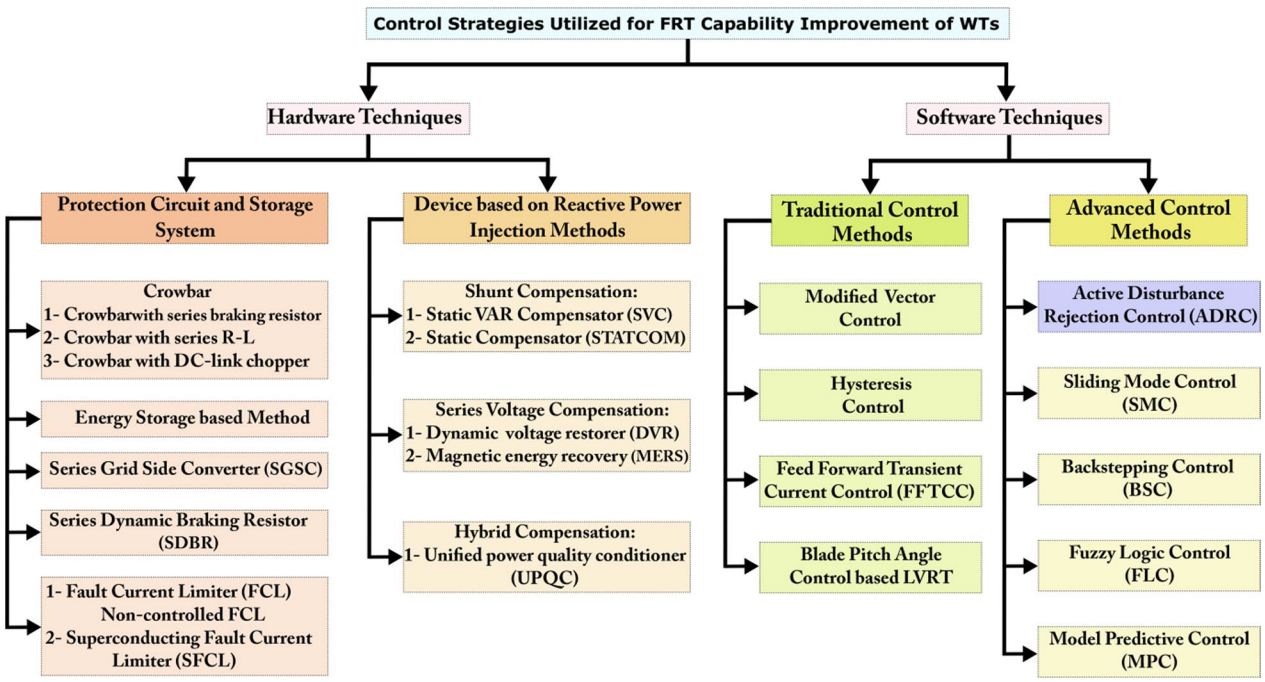

Fig. 1 Classification of FRT capability enhancement Strategies for WTs

power generation systems with different variable-speed WTs technologies. In [9], ADRC is used to control the variable-speed DFIG-based WTs, while in [10], the modeling and robust control of a grid connected direct driven PMSG-based WT using ADRC is presented. In [11] a comparative analysis between PI and ADRC control of a grid connected variable speed wind energy conversion system based on a SCIG is introduced, considering the dynamic behavior of the controller against internal variations in generator parameters.

A large-scale wind farm contains many WTs connected to the grid. The wind farm controller is usually used to provide the maximum power or to guarantee injection of active and reactive power predetermined by the transmission system operator (TSO) and to satisfy the grid code (GC) requirement. However, if a short circuit or a voltage dip occurs in the grid, high transient overcurrent can appear in the WTs. This may exceed the maximum fault current tolerated by the protection system. Consequently, the WTs may have to be disconnected, leading to an imbalance between power consumption and production. In order to ensure power network stability during a grid fault, and to keep the WTs connected to the power network during all operating conditions, it is necessary to develop robust control strategies and efficient supervision configurations for WFs. Therefore, for better management and supervision of WFs, and the current state of the grid and the control mode requested by the TSO (required hourly production), the central supervision unit (CSU) of WFs is configured to control the total active and reactive power exchange with the grid, considering the operating modes such as optimal power control (maximum power point tracking), fault control or PQ control. In addition, the local supervision unit (LSU) of each WT is developed to estimate maximum power capacity, and to collect and send the information of the WTs to the CSU. Thus, to optimally distribute the power production between the different WTs, it must take into consideration the security and reliable operation of the farm. In the literature, several techniques have been investigated toward the design of the supervision algorithms for WFs. Overall, the supervision algorithms can be classified into PI controller (PIC) [12–16], optimization functions (OF) [17–21], and proportional distribution (PD) based [22, 23].

The contribution of this work lies in overcoming the problem of the PCC active and reactive power control. The proposed control strategy for the wind farm is based on the advanced ADRC method combined with the low voltage ride-through control in order to satisfy the GC requirement. This strategy forces a sacrifice of a quantity of active power in order to provide the demanded reactive power, without adding extra devices for reactive power compensation, thus making it more economical. Demonstrations of the three algorithms cited above have shown that the algorithm based on PD is a more attractive choice and thus is adopted in this work in order to distribute the power references proportionally to the WTs. Also, from a security point of view, this algorithm ensures that each WT operates far from its maximum limits.

The remainder of this paper is structured as follows. In Sect. 2, the power supervisory system of a WF is presented, while in Sect. 3, the configuration and modeling of the WF is introduced. The mathematical theory of the ADRC method is presented in Sect. 4. The active and reactive power control of SCIG-based WT is developed in Sect. 5, and Sect. 6 deals with WT control modes during transients. Finally, Sect. 7 presents the validation and simulation results.

2 Supervision algorithms of wind farm active and reactive power

Because of the unforeseeable nature of the primary source of energy, the integration of large capacity WF into a power network has created some challenges to transmission service operators such as stability and reliability of the electrical system, the electrical power quality, and the regulation of voltage and frequency. In order to overcome these problems and to ensure the safety of the power grid, many European countries have recently revised their "grid" regulations. As a result, wind farms are increasingly called upon to comply with the requirements imposed by the grid operator. Thus, recent research on WTs is oriented towards the design of WF supervision algorithms in order to distribute the active and reactive power references over the different WTs of the farm. Sms have been proposed which can be classified mainly into the three groups of PIC, OF, and PD.

2.1 Supervision algorithms based on PI controllers

This algorithm solves the problem of wind farm supervision using a simple PI controller. Two types of algorithms can be adopted, i.e., one uses the PI controller to set the power factor, while the other directly regulates the active and reactive power.

2.1.1 Algorithm for wind farm power factor regulation

In order to control the power factor of the wind farm, this algorithm acts on the reactive power. The reference power factor, derived from the grid operator, is compared to the actual power factor of the farm. A PI type controller with anti-windup is then used to ensure that each WT generates the reference power factor, as discussed in [12, 13]. The block diagram of the wind farm power factor control system is depicted in Fig. 2.

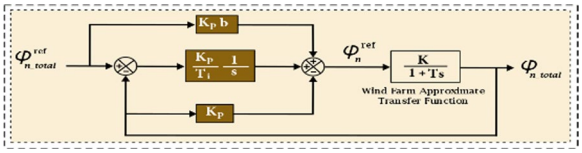

Fig. 2 Simplified block diagram of the wind farm power factor control system [13]

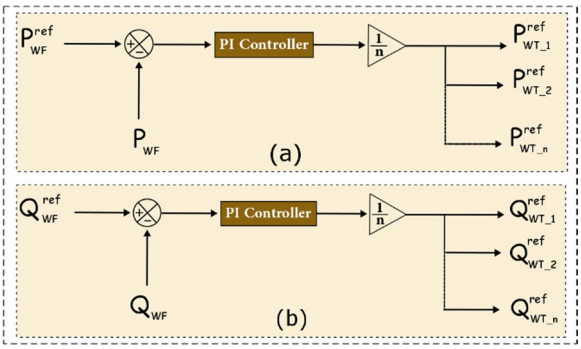

Fig. 3 Power distribution algorithm by PI regulator: **a** active power control, **b** reactive power control

This algorithm has an advantage which lies in the simple and robust adjustment of the power factor and consequently the adjustment of the reactive power. In addition, estimation of the aerodynamic power of each wind generator is not necessary for this supervision algorithm. This facilitates its implementation by reducing the execution time. However, the distribution of the reference reactive power to the WTs of the farm is performed in a non-proportional way, which can cause the saturation of some WTs while others remain capable of providing much more active or reactive power [14].

2.1.2 Algorithm for the regulation of wind farm active and reactive power

Based on the same principle, the algorithm for the distribution of active and reactive power in a wind farm uses a PI controller with anti-windup to control the active and reactive power. During the execution of this algorithm, all the WTs receive the same references from a PI controller that regulates the active and reactive power of the wind farm as reported in [15, 16]. The schematic diagram of this algorithm is shown in Fig. 3.

The advantage of the power distribution algorithm by PI regulator is that it does not require the measurement of the aerodynamic power available at each wind generator. This greatly facilitates the implementation of the algorithm in real time, but the risk of WT saturation is present because the information on the maximum active and reactive power of each turbine is not available and not considered.

2.2 Supervision algorithms based on optimization functions

This category of algorithms uses objective functions for the optimal distribution of active and reactive power of the WTs. The function must formulate the optimization objective by a mathematical equation that takes into account several parameters. Several recent studies have been carried out, and depending on the objective of the algorithm the method can be distinguished into three main types:

1. To minimize the errors between the measured active and reactive power of the farm and their references requested by the transmission system operator as reported in [17].
2. To minimize the errors in the active and reactive power, while considering the minimization of power losses in the lines within the farm in order to optimally exploit the aerodynamic power available at the WTs as shown in [18, 19].
3. To minimize the power losses inside the farm and the deviation of the voltage at the PCC as discussed in [20, 21].

The disadvantage of this method is that a fast supervision algorithm is required, especially an algorithm whose dynamics are higher than the fluctuating production of the farm. This makes the algorithm unusable because its computation time is quite large, which can lead to poor performance when the active and reactive power vary.

2.3 Supervision algorithm based on proportional distribution

Supervision control based on proportional distribution is developed in order to distribute the power proportionally to the WTs. From a safety point of view, this algorithm ensures that each WT will always operate far from its limits defined by the diagram (*P*,*Q*) [22]. This algorithm also determines the active and reactive power references of each WT $P_{wg\_i}^{ref}$ and $Q_{wg\_i}^{ref}$ from the references of the total active and reactive power P_{wf}^{ref} and Q_{wf}^{ref} requested by the grid operator. The production capacity of the active power of the farm is evaluated by summing all available maximum active power at each WT.

The power management algorithm ensures that the power references of the WT ($P_{wg\_i}^{ref}$ and $Q_{wg\_i}^{ref}$) which have the largest production capacity of active power, will have the highest participation rate in wind farm reactive power management. This is because they have the largest reactive power generation or consumption capacity [23].

The expressions of a WT's active and reactive power references are given as:

$$P_{wg\_i}^{ref} = \frac{P_{wg\_i}^{max}}{P_{wf}^{max}} P_{wf}^{ref} \tag{1}$$

$$Q_{wg\_i}^{ref} = \frac{Q_{wg\_i}^{max}}{Q_{wf}^{max}} Q_{wf}^{ref} \tag{2}$$

where $P_{wg\_i}^{max}$ and $Q_{wg\_i}^{max}$ are the maximum active and reactive power of each WT. In the present work the algorithm based on proportional distribution is used.

3 Configuration of wind farm using SCIG

The proposed WT system is depicted in Fig. 4. It consists of three variable speed wind energy conversion systems using SCIGs, each having a power capacity of 2.3 MW. The wind farm is connected to the power grid through cables and overhead transmission lines at the point of common coupling (PCC), and step-up transformers of 0.69/25 kV and 25/125 kV.

The detailed WT model is composed of a three-bladed rotor, a mechanical gearbox, a SCIG with a fully rated back-to-back converter (stator and grid side converters), DC link capacitor and a line filter. The WT system converts variable mechanical power to variable electrical power to the grid, and two controls are adopted (stator side and grid side) using the ADRC controllers with pitch control, as illustrated in Fig. 8. However, to further study the proposed system performance, the system is modeled in the grid *dq*-synchronous reference frame. The power system data is summarized in ``Appendices 1 and 2".

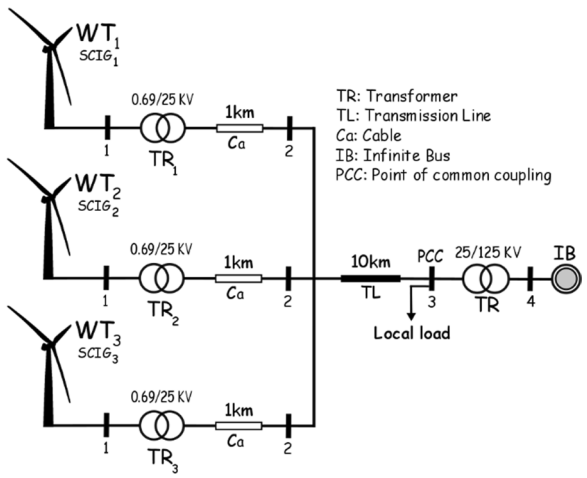

Fig. 4 Global scheme of SCIG-based WF connected to the grid proposed

3.1 Mechanical dynamic model

The mechanical model of the WT system has been discussed in other work [11, 23], and thus is only briefly presented here. The mechanical power available from the WT rotor depends on the WT aerodynamic behavior and is given by:

$$P_{aero} = C_p(\lambda, \beta) P_w = C_p(\lambda, \beta) \frac{1}{2} \rho A_{wt} w_{t\_i}^3 \tag{3}$$

where P_w is the kinetic power from wind, C_p is the energy coefficients which depend on the blade pitch angle β and turbine tip speed ratio λ. A_{wt}, ρ and w_{t_i} are the turbine blades area, air density and wind speed of the ith WT, respectively. The expression for the turbine tip speed ratio is given by:

$$\lambda = \frac{R\Omega_{tur\_i}}{w_{t\_i}} \tag{4}$$

where Ω_{tur_i} is the turbine speed, and R is the turbine blade radius.

3.2 SCIG dynamic model

For the modeling of the electrical generator, it is assumed that the stator and rotor windings are placed sinusoidally and symmetrically, and the magnetic saturation effects of all the windings are negligible [9]. SCIG is represented by:

$$\begin{bmatrix} v_{sd} \\ v_{sq} \\ 0 \\ 0 \end{bmatrix} = [R_{sr}] \begin{bmatrix} i_{sd} \\ i_{sq} \\ i_{rd} \\ i_{rq} \end{bmatrix} + \frac{d}{dt} \begin{bmatrix} \Psi_{sd} \\ \Psi_{sq} \\ \Psi_{rd} \\ \Psi_{rq} \end{bmatrix} + [\omega_{sr}] \begin{bmatrix} \Psi_{sd} \\ \Psi_{sq} \\ \Psi_{rd} \\ \Psi_{rq} \end{bmatrix} \tag{5}$$

with

$$[R_{sr}] = \begin{bmatrix} -R_s & 0 & 0 & 0 \\ 0 & -R_s & 0 & 0 \\ 0 & 0 & -R_r & 0 \\ 0 & 0 & 0 & -R_r \end{bmatrix}$$

$$[\omega_{sr}] = \begin{bmatrix} 0 & -\omega_s & 0 & 0 \\ \omega_s & 0 & 0 & 0 \\ 0 & 0 & 0 & -s\omega_s \\ 0 & 0 & s\omega_s & 0 \end{bmatrix}$$

where i, v and Ψ are the current, voltage and field flux linkage, respectively. L and R are the inductance and resistance. The subscripts s and r indicate the stator and rotor of the generator, and ω_s is the electrical angular speed.

The stator and rotor magnetic field equations are:

$$\begin{bmatrix} \Psi_{sd} \\ \Psi_{sq} \\ \Psi_{rd} \\ \Psi_{rq} \end{bmatrix} = \begin{bmatrix} -L_s & 0 & L_m & 0 \\ 0 & -L_s & 0 & L_m \\ L_m & 0 & -L_r & 0 \\ 0 & L_m & 0 & -L_r \end{bmatrix} \begin{bmatrix} i_{sd} \\ i_{sq} \\ i_{rd} \\ i_{rq} \end{bmatrix} \quad (6)$$

where $L_s = L_m + L_{s\sigma}$ and $L_r = L_m + L_{r\sigma}$, with $L_{s\sigma}$, $L_{r\sigma}$ and L_m being the stator leakage inductance, rotor leakage inductance and mutual inductance, respectively.

The expression for the electrical active and reactive power delivered by the generator (P_s, Q_s) is:

$$\begin{bmatrix} P_s \\ Q_s \end{bmatrix} = \frac{3}{2} \begin{bmatrix} \mathrm{v}_{sd} & \mathrm{v}_{sq} \\ \mathrm{v}_{sq} & -\mathrm{v}_{sd} \end{bmatrix} \begin{bmatrix} i_{sd} \\ i_{sq} \end{bmatrix}. \quad (7)$$

3.3 Line-side converter, transformer and cable dynamic models

As reported in [23], the magnetization parameters of the transformer (resistance and reactance) and cable capacitance have large impedance. The models of the filter, transformer and cable are illustrated in Fig. 5, and their mathematical models in the d–q frame are represented as follows.

3.3.1 Line-side converter model

The WT is connected to the grid through an *RL* filter, and the model of the filter-side can be expressed as:

$$\begin{bmatrix} \mathrm{v}_{fd} \\ \mathrm{v}_{fq} \end{bmatrix} = [L_f] \frac{d}{dt} \begin{bmatrix} i_{fd} \\ i_{fq} \end{bmatrix} - [M_f] \begin{bmatrix} i_{fd} \\ i_{fq} \end{bmatrix} + \begin{bmatrix} v_{id} \\ v_{iq} \end{bmatrix} \quad (8)$$

with $[L_f] = \begin{bmatrix} -L_f & 0 \\ 0 & -L_f \end{bmatrix}$ and $[M_f] = \begin{bmatrix} R_f & -\omega_e L_f \\ \omega_e L_f & R_f \end{bmatrix}$

where v_{fd} and v_{fq} are the filter output voltage components in d–q frame, i_{fd} and i_{fq} are the filter current components, and v_{id} and v_{iq} are the inverter output voltage components in d–q frame. R_f and L_f are the resistance and inductance of the filter, respectively.

3.3.2 Transformer dynamic model

The mathematical model of the transformer in the d–q synchronous reference frame is expressed as [24]:

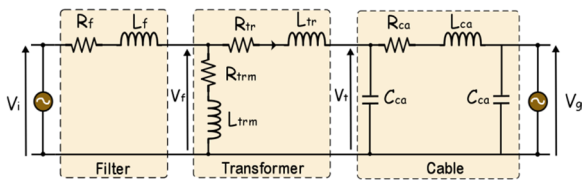

Fig. 5 Scheme simplified model of the filter, the transformer and the cable

$$\begin{bmatrix} \mathrm{v}_{td} \\ \mathrm{v}_{tq} \end{bmatrix} = [L_{tr}] \frac{d}{dt} \begin{bmatrix} i_{gd} \\ i_{gq} \end{bmatrix} - [M_{tr}] \begin{bmatrix} i_{gd} \\ i_{gq} \end{bmatrix} + \begin{bmatrix} v_{fd} \\ v_{fq} \end{bmatrix} \quad (9)$$

with $[L_{tr}] = \begin{bmatrix} L_{tr} & 0 \\ 0 & L_{tr} \end{bmatrix}$ and $[M_{tr}] = \begin{bmatrix} R_{tr} & -\omega_e L_{tr} \\ \omega_e L_{tr} & R_{tr} \end{bmatrix}$

where v_{td} and v_{tq} are the transformer output voltage components in d–q frame, and i_{gd} and i_{gq} are the d–q grid current components. R_{tr} and L_{tr} are the resistance and inductance of the transformer, respectively.

3.3.3 Cable dynamic model

As discussed in [24], the cable dynamic model in the d-q frame is represented by:

$$\begin{bmatrix} \mathrm{v}_{gd} \\ \mathrm{v}_{gq} \end{bmatrix} = [L_{ca}] \frac{d}{dt} \begin{bmatrix} i_{gd} \\ i_{gq} \end{bmatrix} - [M_{ca}] \begin{bmatrix} i_{gd} \\ i_{gq} \end{bmatrix} + \begin{bmatrix} v_{td} \\ v_{tq} \end{bmatrix} \quad (10)$$

with $[L_{ca}] = \begin{bmatrix} L_{ca} & 0 \\ 0 & L_{ca} \end{bmatrix}$ and $[M_{ca}] = \begin{bmatrix} R_{ca} & -\omega_e L_{ca} \\ \omega_e L_{ca} & R_{ca} \end{bmatrix}$

where v_{gd} and v_{gq} are the d–q components of the grid voltage, and i_{gd} and i_{gq} are the d–q components of the grid current. R_{ca} and L_{ca} are the resistance and inductance of the cable, respectively.

The WT active and reactive power (P_{wg}, Q_{wg}) injected into the grid are given by:

$$\begin{bmatrix} P_{wg} \\ Q_{wg} \end{bmatrix} = \frac{3}{2} \begin{bmatrix} \mathrm{v}_{gd} & \mathrm{v}_{gq} \\ \mathrm{v}_{gq} & -\mathrm{v}_{gd} \end{bmatrix} \begin{bmatrix} i_{gd} \\ i_{gq} \end{bmatrix}. \quad (11)$$

4 Mathematical modeling of the ADRC method

4.1 Active disturbance rejection control

Most real systems are not only non-linear and varying in time, but also uncertain with variations in the parameters described in their mathematical models. The ADRC controller overcomes the shortcomings of the conventional controllers such as RST, PI, PID controllers etc. To illustrate the principle of the ADRC technique, a single-input, single-output non-linear time-varying object is considered [25]:

$$\begin{cases} x^n = f\left(x, \dot{x}, \cdots, x^{n-1}, d, t\right) + b.u \\ x = y \end{cases} \quad (12)$$

where $x, \dot{x}, \cdots, x^n$ represent the respective object state and its various order dynamics. d is the external disturbances, and $f\left(x, \dot{x}, \cdots, x^{n-1}, d, t\right)$ represents all internal and external disturbances (total disturbances) affecting the system to be controlled. u and y are the system input and output, respectively, and b is the control gain.

The advantage of ADRC is that even if the dynamic model of the system is not clear and there is large uncertainty in the control gain, good control performance can still be obtained. The basic structure of the ADRC controller is shown in the block diagram in Fig. 6. It consists

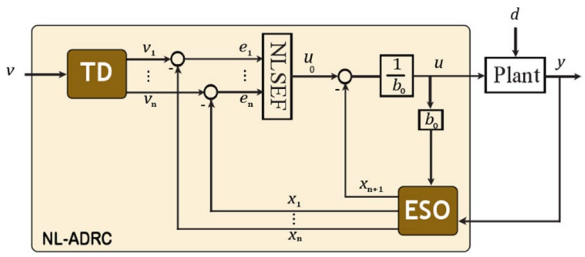

Fig. 6 Block diagram of an n-order nonlinear ADRC

of three parts which can have many different forms, i.e., the Tracking Differentiator (TD), Extended State Observer (ESO) and Non-Linear State Error Feedback (NLSEF). If each part of the ADRC contains a nonlinear link, it is called a nonlinear ADRC; otherwise, it is called a linear ADRC [26]. The principles of the three parts are introduced below. Among them, b_0 is the estimated value of b, which can also be adjusted according to the control needs and also be adaptive online.

For the ADRC shown in Fig. 6, v and v_1 are the input and input tracking signals, respectively. y is the system feedback signal, and x is the estimated tracking signal. b_0 is the compensation factor, and x_2/b_0 is the internal and external disturbances compensation. u_0 is the initial control object by NLSEF, and u is the final control signal after disturbance compensation.

4.1.1 Tracking differentiator (TD)

To avoid a sudden jump of the control signal and to track the transient profile of the reference signal to resolve the problem of set-point jump in the traditional PID controller, a tracking differentiator (transient profile generator) is used to arrange the transition of a given signal according to the input limit of the controlled object. While obtaining a smooth input, it also provides the differential signal of each order of the input. The general form of a continuous nonlinear tracking differentiator of a nth-order uncertain system is [26]:

$$\begin{cases} \dot{v_1} = v_2 \\ \dot{v_2} = v_3 \\ \vdots \\ \dot{v_n} = \gamma^n f\left(v_1 - v, \frac{v_2}{\gamma}, \cdots, \frac{v_n}{\gamma^{n-1}}\right) \end{cases} \tag{13}$$

where v is the TD input signal, v_i are the TD output signals which are the tracking signals of the input v with $i = 1, 2, \cdots, n$. The coefficient γ is called the speed factor, and the larger it is, the faster v_i tracks the input signal v.

4.1.2 Extended state observer ESO

Most control systems can react promptly to changes in the internal dynamics of the plant and external disturbances. Thus, in the ADRC framework, the extended state observer is the core of the entire controller. It not only undertakes the task of estimating the state variables of the system and their deferential signals of various orders, but also accurately comprehends the overall disturbances and cancels in the control law, even with the absence of an accurate mathematical model of the system. The ESO can be classified into two types, i.e., linear and nonlinear according to the error correcting terms including the function of the error [27].

Then, it is assumed that the system dynamic model is completely unknown, and the total disturbances are estimated in real-time through the extended state. The general form of designing a continuous, extended state observer is:

$$\begin{cases} e = x_1 - y \\ \dot{x}_1 = x_2 - \beta_{01} \cdot g_1(e) \\ \dot{x}_2 = x_3 - \beta_{02} \cdot g_2(e) \\ \vdots \\ \dot{x}_n = x_{n+1} - \beta_{0n} \cdot g_n(e) + b_0 \cdot u \\ \dot{x}_{n+1} = -\beta_{0(n+1)} \cdot g_{n+1}(e) \end{cases} \tag{14}$$

where x_i are the estimated values of states y_i and the total disturbances x_{n+1}, β_{0i} are the observer adjustable gains, and $g_i(e)$ is a nonlinear constructed function.

For the specific design of an ESO, a large number of existing observer and filter design techniques can be used. $g_i(e)$ is chosen as the specific nonlinear function, which has the form of [28]:

$$fal(e, a_i, \delta) = \begin{cases} |e|^{a_i} sgn(e) |e| > \delta \\ \frac{e}{\delta^{1-a_i}} |e| \le \delta \end{cases} \tag{15}$$

Thus, the ESO can estimate the state of the object and the total disturbance of the system with a certain accuracy, as:

$$x_1 \to y_1, \cdots, x_n \to y_n, x_{n+1} \to f(\cdot). \tag{16}$$

4.1.3 State error feedback control law

The ADRC approach is a combination of obtaining the best estimation value of the total disturbance by ESO, and its compensation in real time by the control law. Therefore, the control law is taken as [29]:

$$u = \frac{u_0 - x_{n+1}}{b_0} \tag{17}$$

where u_0 is the initial control signal for the already disturbance-free system designed to meet some predefined closed-loop requirements, and x_{n+1} is the estimation of the unknown total disturbance.

While it is temporarily assumed that the estimation loop is well tuned ($x_{n+1} = f(.)$), the proposed control law can be incorporated in the extended system in each control cycle theoretically as:

$$y^n = f(\cdot) + b_0 \frac{u_0 - x_{n+1}}{b_0} \approx u_0 \tag{18}$$

At the same time the controlled objects that are full of disturbances, uncertainties and nonlinearities are uniformly converted into standard integrator types. This makes the design of the control system simple and intuitive, and has broad applicability.

The general form of the Nonlinear State Error Feedback (NLSEF) control law for controlled objects of n-order is given by:

$$u_0 = \sum_{i=1}^{n} k_i fal\left(e_i, a'_i, \delta'\right) \tag{19}$$

where $e_i = v_i - x_i$, k_i is the gain coffecient, a'_i and δ' are undetermined constants, usually chosen as $0 < a'_i < 1 < a'_i$ $(i = 1, 2, \ldots, n)$, In this way, the differential effect will become smaller when it is close to the steady state. This helps to improve the performance of the control system [30].

Ultimately, when $a'_i = 1$, the control law becomes linear. The advantage of a linear control law is that parameter tuning is simple and the control effect is relatively smooth. In this paper the linear-ADRC is adopted and used to control the SCIG-based wind farm.

4.2 Linear-ADRC design

As indicated in the previous sections, the ADRC control technologies can be divided into linear and non-linear strategies, the latter because of the usage of nonlinear functions in all three parts of the ADRC. Considering the difficulties in practical application, the linear-ADRC control technology, which was proposed in [31] with its basic idea of selecting the parameters of the ADRC controller based on the bandwidth, is used in this paper. Bandwidth is a performance index of control system response, and the higher it is, the better the immunity is. Thus, when designing the controller and the extended state observer parameters, the bandwidth can be used as the only tunable parameter of the system, and the remaining parameters are converted into functions of the bandwidth.

To illustrate the detailed principle of the linear-ADRC, the dynamic *n*th-order system is considered as represented by [29]:

$$y^{(n)} = f(\mathrm{y}, \mathrm{u}, \mathrm{d}) + b_0.u \tag{20}$$

where y is the system output, f and d are the total and external disturbances, and u and b_0 are the signal and gain of the control.

Assuming that f is differentiable with $h = \dot{f}$, (20) can be written in the state space form as:

$$\begin{cases} \dot{x} = Ax + Bu + Dh \\ y = Cx \end{cases} \tag{21}$$

with:

$$x = [x_1, x_2, \ldots., x_{n-1}, x_n, x_{n+1}]^T$$

$$A_{(n+1,n+1)} = \begin{bmatrix} 0 & 1 & 0 & \cdots & 0 \\ 0 & 0 & 1 & \cdots & 0 \\ \vdots & & & \ddots & \vdots \\ 0 & 0 & 0 & & 1 \\ 0 & 0 & 0 & \cdots & 0 \end{bmatrix}$$

$$B_{(n+1,1)} = [\,0\ 0\ \cdots\ b_0\ 0\,]^T$$

$$C_{(1,n+1)} = \begin{bmatrix} 1\ 0\ \cdots\ 0\ 0 \end{bmatrix}$$

$$D_{(n+1,1)} = [\,0\ 0\ \cdots\ 0\ 1\,]^T$$

A full-order Luenberger state-observer can be designed as:

$$\begin{cases} \dot{\widehat{x}} = A\widehat{x} + Bu + L_{obs}(y - \widehat{y}) \\ \widehat{y} = C\widehat{x} \end{cases} \tag{22}$$

where L_{obs} represents the observer gains vector, and $L_{obs} = \left[\beta_{01}\beta_{02}\cdots\beta_{0n}\beta_{0(n+1)}\right]^T$.

The error obtained by ESO between the actual x and estimated $\widehat{x}$ is given by:

$$\varepsilon = x - \widehat{x} \tag{23}$$

Therefore, the error estimation dynamics are expressed by:

$$\dot{\varepsilon} = (A - L_{obs}C)\varepsilon \tag{24}$$

where

$$A - L_0C = \begin{bmatrix} -\beta_{01} & 1 & 0 & & \cdots & 0 \\ -\beta_{02} & 0 & 1 & & & 0 \\ \vdots & & & & \ddots & \vdots \\ -\beta_{0n} & & 0 & 0 & & 1 \\ -\beta_{0(n+1)} & & 0 & 0 & \cdots & 0 \end{bmatrix}$$

To guarantee good functioning of the estimation ($\varepsilon \to 0$), the parameters of the gain matrix L_{obs} must be chosen such that $(A - L_{obs}C)$ forms a Hurwitz matrix, i.e., the poles of its polynomial characteristic $P_{obs}(s)$ are all with strictly negative real parts [31].

$$P_{ESO}(s) = \det(sI_{n+1} - (A - L_{\text{obs}}C)) \tag{25}$$

Then, the polynomial characteristic $P_{obs}(s)$ is:

$$P_{ESO}(s) = s^{(n+1)} + \beta_1 s^{(n)} + \beta_2 s^{(n-1)} + \cdots + \beta_{(n+1)} \tag{26}$$

Generally, the pole placement technique is used to determine the observer's gains. A compromise must be established between the observer tracking speed and its noise measurement sensitivity. As ESO becomes faster, the disturbance is estimated early and then cancelled by the controller. This process is achieved by positioning the observer poles just to the left of the observed process poles in the *P*-plan. Such choice leads to the adoption of a large bandwidth for ESO. However, it should be noted that, as the bandwidth becomes larger, the system can be harmed by promoting noise transmission [32].

$$P_{ESO}(s) = (s + \omega_{obs})^{n+1} \tag{27}$$

The generally expression of observer gains is then:

$$\beta_{0i} = \frac{(n+1)!}{(n+1-i)!i!}\omega_{obs}^{i} \tag{28}$$

The linear observer gains are:

$$\beta_1 = 2\omega_{obs};\ \beta_2 = \omega_{obs}^2 \tag{29}$$

As a result, when $(A - L_{obs}C)$ is stable, $\widehat{x}_1, \widehat{x}_2, \cdots, \widehat{x}_n$ will approximate $y_1, y_2, \cdots, y_n$ and the derivatives (up to order n-1), and $\widehat{x}_{n+1}$ will approximate the total disturbance $f(y, u, d)$. Consequently, the final control amount can take into consideration the estimated disturbances and reject them in real time.

If the final control law is chosen as:

$$u = \frac{u_0 - \widehat{x}_{n+1}}{b_0} \tag{30}$$

the system equation in (20) becomes:

$$y^{(n)} = f(\mathrm{y}, \mathrm{u}, \mathrm{d}) - \widehat{x}_{n+1} + u_0 \tag{31}$$

For a good estimation of generalized disturbance ($\widehat{x}_{n+1} \approx f(y, u, d)$), the system is:

$$y^{(n)} = u_0 \tag{32}$$

To effectively implement the control to reject disturbance, the actual state-feedback control law is designed by:

$$u_0 = k_1(r - y) + k_2(\dot{r} - \dot{y}) + \cdots + k_n\left(r^{(n-1)} - y^{(n-1)}\right) \tag{33}$$

where r is the reference signal.

Since $\widehat{x}_1, \widehat{x}_2, \cdots, \widehat{x}_n$ are the correct estimation of $y, \cdots, y^{(n-1)}$, the final control law can be approximated as:

$$u = \frac{1}{b_0}\left[k_1(r - \widehat{x}_1) + \cdots + k_n\left(r^{(n+1)} - \widehat{x}_n\right) - \widehat{x}_{n+1}\right] \tag{34}$$

and

$$u = K_0(\widehat{r} - \widehat{z}) \tag{35}$$

where

$$\widehat{r} = [\, r \ \dot{r} \ \cdots \ r^{(n+1)} \ 0 \,]^T \tag{36}$$

$$K_0 = \frac{[\, k_1 \ k_2 \ \cdots \ k_n \ 1 \,]}{b_0} \tag{37}$$

The linear-ADRC can be summarized and designed by:

$$\begin{cases} \dot{\widehat{x}} = (A - L_{\text{obs}}C)\widehat{x} + Bu + L_{\text{obs}}y \\ u = K_0(\widehat{r} - \widehat{z}) \\ \widehat{x}_1 = \widehat{y} \, and \, \widehat{x}_2 = \widehat{f} \end{cases} \tag{38}$$

The structure of a first order linear-ADRC approach is displayed in Fig. 7.

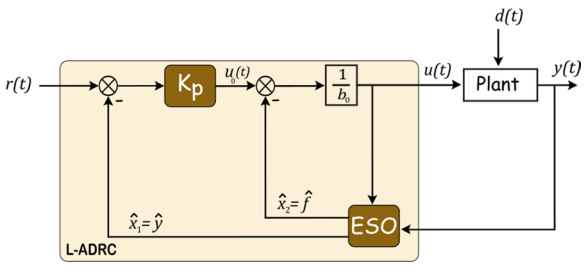

Fig. 7 Block diagram of a linear-ADRC structure [11]

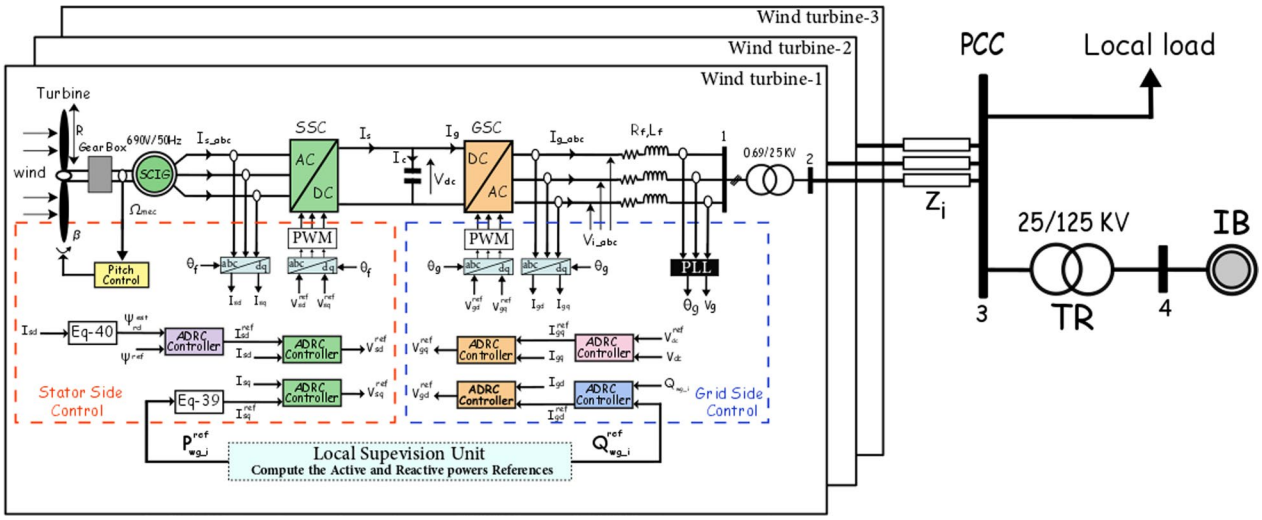

Fig. 8 Global scheme ADRC Strategy control of a SCIG-based WF

5 Wind turbine system control strategy by linear ADRC

This section deals with the proposed control strategy of a WT, while its objectives are the control of the active power and the generator magnetization, and the reactive power at the PCC. The ADRC control strategy is used here and since a non-linear ADRC strategy needs to adjust a large number of parameters—which is complicated and also increases the model complexity [10]—a linear-ADRC control design is applied.

The global scheme of a WT system using the ADRC control strategy is depicted in Fig. 8. In order to control the stator-side converter (SSC) and grid-side converter (GSC), the indirect rotor field oriented control ($\Psi_{rd} = \Psi_r$,$\Psi_{rd} = 0$) and voltage oriented control ($v_{gd} = 0, v_{gq} = V_g$) are applied, respectively. However, the main objective of the stator-side converter is to force the states of the wind system to track their desired references, or in such a way to regulate the stator power to the given reference by the LSU and to regulate the rotor field to track the rated value. In addition, the grid side converter is used to control the active power injected into the utility grid through the regulation of the DC link voltage, and to control the reactive power exchanged with the power grid at PCC.

The reference current i_{sq}^{ref} is calculated by the desired delivery of active power, as:

$$i_{sq}^{ref} = \frac{L_r}{L_m \Psi^{ref} \omega_{mec}} P_{wg\_i}^{ref} \tag{39}$$

where $P_{wg\_i}^{ref}$ and $Q_{wg\_i}^{ref}$ are the references power imposed by the LSU.

The rotor field estimation is given by:

$$\Psi^{est} = \frac{L_m}{1 + \frac{R_r}{L_r} s} i_{sd}. \tag{40}$$

where s is the Laplace operator.

To limit the extracted power and the turbine speed, a blade orientation system is used to adjust the blade pitch angle as shown in Fig. 8. The choice of the reference angle generally comes from an external loop which is used to regulate the turbine speed and the generated mechanical power [33].

5.1 Remark

The control by ADRC of SCIG-based WT and its design for both the stator and grid side converters (except the grid reactive power regulator) are presented in detail in [11], in which a comparative analysis between PI and ADRC controllers for the SCIG-based WT is given.

To achieve an effective regulation of the reactive power problem at the PCC, it is necessary to control the reactive power of each WT. This can be achieved by the ADRC controller. As a result, to design the ADRC regulator of reactive power control, it needs to establish the control loops, the transformer and the transmission cable dynamic model [23]. The regulation of the grid reactive power is then achieved by adopting a linear-ADRC controller, wherein its canonical form is given by:

$$\dot{y}(t) = f\left(y, u, d\right) + b_0 u(t) \tag{41}$$

where $f\left(y, u, d\right)$ represents the total (internal and external) disturbance, b_0 is the known part of the process

(system), d represents the external disturbance, and $u(t)$ and $y(t)$ are the input and output of the process, respectively.

The orientation of grid voltage on the q-axis is achieved by the phase locked loop (PLL) in order to obtain $v_{gd} = 0, v_{gq} = V_g$. The reactive power of the WT can be written as:

$$Q_{wg} = \frac{3}{2} V_g i_{gd} \tag{42}$$

According to (8)–(10) and (42), the expression of the change of reactive power exchange with the grid can be given by:

$$\frac{d}{dt} Q_{wg} = -\frac{3}{2}\frac{R}{L} V_g i_{fd} - \frac{3}{2}\omega_e V_g i_{fq} - v_{fd} \tag{43}$$

where $R = R_{tr} + R_{ca}$ and $L = L_{tr} + L_{ca}$.

Therefore, the linear-ADRC design for reactive power regulation, after adaptation of the exchange reactive power with the grid equation to the ADRC canonical form, is:

$$\begin{cases} f_{Q_{wg}} = -\frac{3}{2}\omega_e V_g i_{fq} - v_{fd} + \left(-\frac{3}{2}\frac{R}{L} V_g - b_0^{Q_{wg}}\right) i_{fd} \\ b_0^{Q_{wg}} = -\frac{3}{2}\frac{R}{L} V_g \\ u_{Q_{wg}} = i_{fd} \end{cases} \tag{44}$$

where $f_{Q_{wg}}$ is the total (external and internal) disturbances affecting the reactive power, and $b_0^{Q_{wg}}$ are the known parts of the system parameters.

6 Supervisory and management system of the wind farm

To overcome the stability, power quality and reliability problems of an electrical power system, and for better supervisory and management system of the wind farm, a central wind farm supervisory unit is set up to monitor the total active and reactive power (P_{wf}, Q_{wf}) that is exchanged between the wind farm and the power grid. In this way, the CSU receives an hourly production plan of the active and reactive power references demanded from the transmission system operator (P_{wf}^{ref}, Q_{wf}^{ref}), and also provides the TSO with information about the total maximum power that can be generated by the wind farm (P_{wf}^{max}, Q_{wf}^{max}).

Subsequently, by using the proportional distribution algorithm rule, the WF CSU will output in real time the active and reactive power references of each wind generator ($P_{wg\_i}^{ref}$,$Q_{wg\_i}^{ref}$) to the LSU. In contrast, according to the current state of the power network and the control mode requested by the TSO such as MPPT control mode, fault control mode or PQ control mode, LSU estimates and sends the maximum capacity of active/reactive power production of the different wind turbines to the CSU ($P_{wg\_i}^{max}$,$Q_{wg\_i}^{max}$).

The supervisory and the management of the power system configuration of the WF based on an SCIG generator is depicted in Fig. 9.

The maximum active and reactive power capacity of the farm can be estimated by the sum of the maximum active and reactive power available from each of the WTs:

$$P_{wf}^{max} = \sum_{i=1}^{n} P_{wg\_i}^{max} \tag{45}$$

$$Q_{wf}^{max} = \sum_{i=1}^{n} Q_{wg\_i}^{max} \tag{46}$$

where $P_{wg\_i}^{max}$ and $Q_{wg\_i}^{max}$ are the maximum active and reactive power of the ith WT, respectively, and n is the number of WTs in the farm.

The maximum active power available from the ith WT and the maximum reactive power that can be exchanged by the line-side converter and the grid can be expressed respectively as:

$$P_{wg\_i}^{max} = P_{opt\_i} \tag{47}$$

$$Q_{wg\_i}^{max} = \sqrt{S_{wg\_i}^2 - P_{wg\_i}^{max2}} - Q_{s\_i} \tag{48}$$

where S_{wg_i} is the nominal apparent power of the ith WT.

The LSU of each WT generates the necessary active and reactive power references, according to one of the three management modes (MPPT, Fault or PQ) which are developed subsequently.

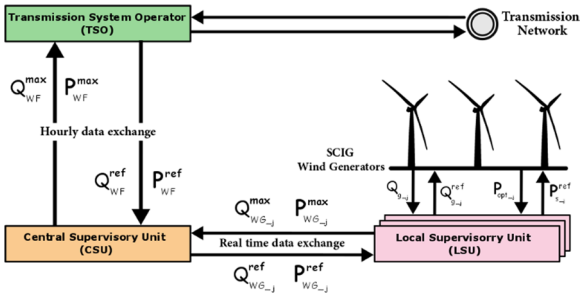

Fig. 9 Schematic diagram of the supervision power system configuration

6.1 Optimal power control (or MPPT) mode

In the normal case without grid fault ($V_{g_{pu}} > 0.9$), the wind energy conversion system will be controlled by the Optimal Power Control (OPC) algorithm to extract

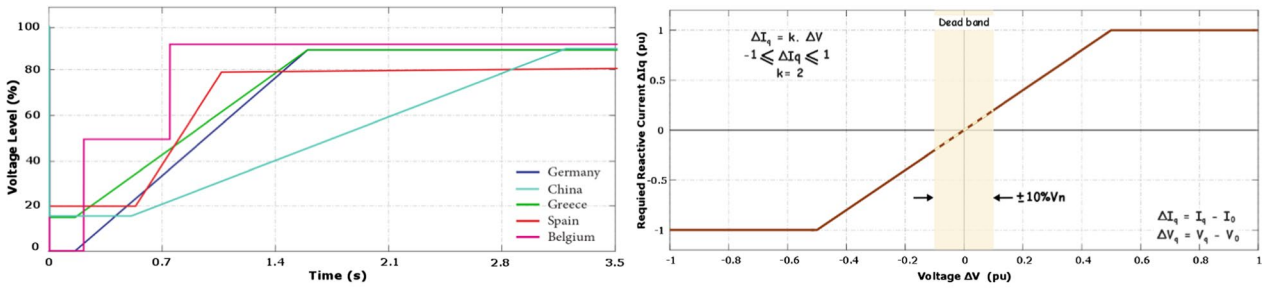

Fig. 10 Grid code requirements: **a** voltage drop (LVRT) profile, **b** reactive current injection in the German grid code [34]

the maximum power from the WT. In order to capture the maximum available power from the turbine, the rotor mechanical speed is adjusted through the electromagnetic torque to maintain the tip speed ratio at its optimum value ($\lambda = \lambda^{opt}$) and the power coefficient ($C_p = C_p^{max}$) for a given value of blade pitch angle $\beta = 0°$.

The optimal aerodynamic power is then given by:

$$P_{opt\_i} = \frac{1}{2}\rho\pi R^5 \frac{C_p^{max}}{\lambda^{opt3}} \frac{1}{p^3 G^3} \omega_{mec\_i}^3 \tag{49}$$

where ω_{mec_i} represents the mechanical angular speed of the ith WT.

The reference of the stator power in this mode is:

$$P_{wg\_i}^{ref} = P_{opt\_i} = K_{opt}\omega_{mec\_i}^3 \tag{50}$$

where the optimal power coefficient K_{opt} is:

$$K_{opt} = \frac{1}{2}\rho\pi R^5 \frac{C_p^{max}}{\lambda^{opt3}} \frac{1}{p^3 G^3} \tag{51}$$

The reference of the grid reactive power is set to zero for a unit power factor:

$$Q_{wg\_i}^{ref} = 0. \tag{52}$$

6.2 Fault control mode

Grid connected wind generation systems can have negative impacts on the power network especially for large systems. When a voltage dip occurs in the grid ($V_{g_{pu}} \leq 0.9$), the WT system could become unstable resulting in it being disconnected from the network. Therefore, to mitigate the negative impacts on the grid, grid codes in many countries require the system to remain connected to the grid when the voltage drops for a specified time, while supporting the grid with reactive current injection (LVRT requirements). Figure 10a presents the grid code requirements for different countries, while for the German grid code, the curve of the reactive current supplied by the WT versus the voltage drop for LVRT control is depicted in Fig. 10b. As shown in Fig. 10b, each percentage of voltage drop requires a 2% slope of positive reactive current injection. When the voltage sag value is higher than 50%, the injection of reactive current goes to 100% or higher depending on the inverter's rated current.

According to the German grid code, the reference of the reactive current to be injected into the grid versus the magnitude of the voltage during the fault is given as [35]:

$$I_r^{ref} = \begin{cases} k\left(1 - V_{g_{pu}}\right) I_{r_n} if 0.9 \geq V_{g_{pu}} > 0.5 \\ I_{r_n} if V_{g_{pu}} \leq 0.5 \end{cases} \tag{53}$$

where I_r^{ref} is the reference reactive current, I_{r_n} is the nominal reactive current, $V_{g_{pu}}$ is the per unit value of the grid voltage during the disturbance, and k is a constant value which equals 2 in this paper.

Consequently, the expression of supplied reactive power versus the magnitude of the grid voltage is determined by:

$$Q_{LVRT}^{ref} = \frac{3}{2} V_g I_r^{ref} \tag{54}$$

Under fault operation, it is necessary to reduce the active power transferred from the WT system in order not to exceed the rated apparent power S_{wg_i}. Therefore, the active power reference is calculated using the reactive power reference ($Q_{g\_i}^{ref}$) and the rated apparent power of the ith WT, as:

$$P_{wg\_i}^{ref} = \sqrt{S_{wg\_i}^2 - Q_{wg\_i}^{ref\ 2}}. \tag{55}$$

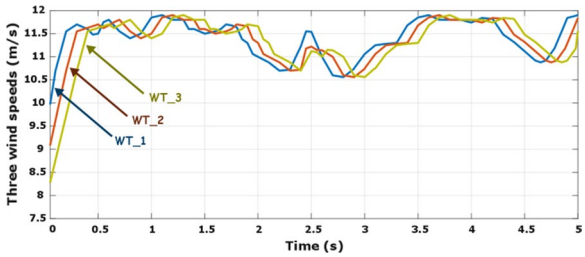

Fig. 11 Wind speed profiles

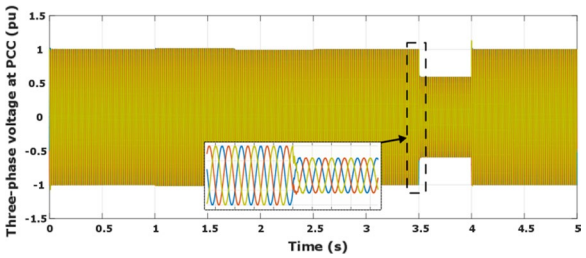

Fig. 13 Three phase voltage of grid

6.3 PQ control mode

The PQ control mode is used to force the wind farm to generate the maximum capacity or lower of the active power production, through stator side converter control. In addition, the grid side converter is used to control the active power injected into network and the required reactive power by TSO.

As indicated previously, the proportional distribution power management algorithm is used to ensure that the power references of the WT that have the largest active power production and reactive power generation or consumption capacities, have the highest participation rate in wind farm reactive power management [11].

The expression of a WT's active and reactive power references for this mode are given in (1) and (2). In contrast, if the required reactive power has priority over the generated reactive power, the wind farm must sacrifice a quantity of active power to satisfy the reactive power demand under some conditions. For the first case, the reactive power reference imposed by the supervisory system should not exceed the maximum value given in (48), while in the second, the expression of the active power reference is given in (55).

Finally, in order to set up the supervision algorithm of SCIG-based wind farm, the control algorithm that must be followed is summarized and presented in "Appendix 2".

7 Simulation results and discussion

The full model of the wind farm and the grid, and its supervisory control system illustrated in Fig. 4 is established using the Matlab/Simulink environment. In order to validate the WF control strategies described in the previous sections, the model consists of three SCIG-based WTs connected to PCC with a total capacity of 6.9 MW. The simulation parameters are given in "Appendix 1", and the three different wind

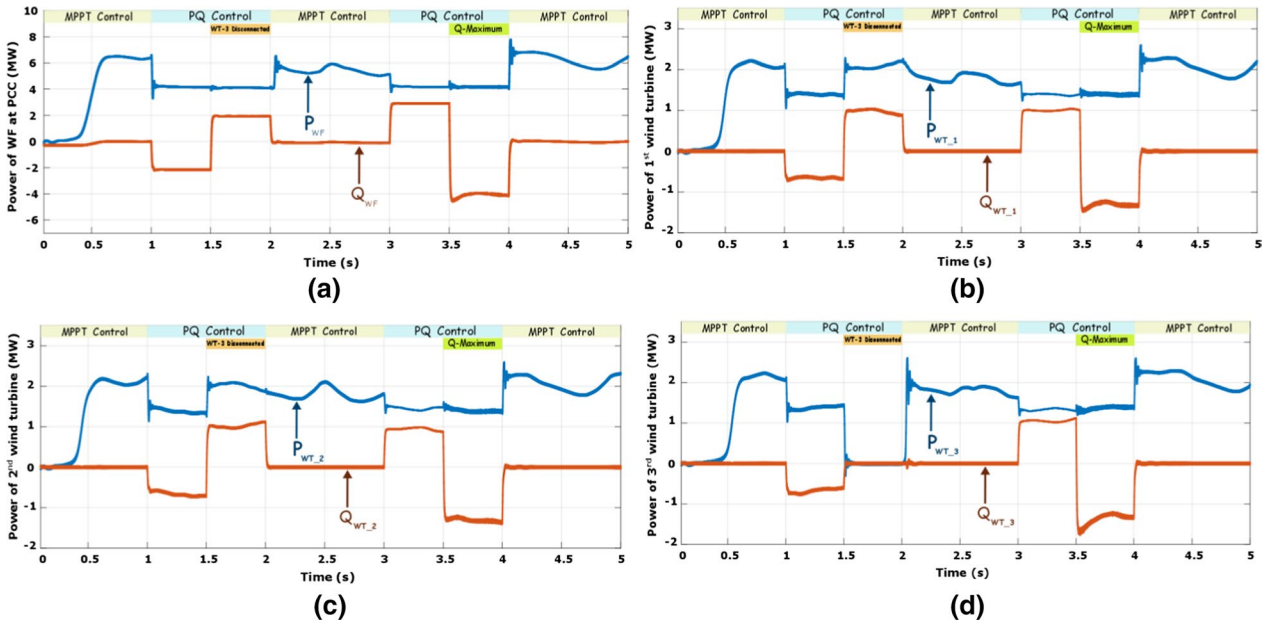

Fig. 12 Simulation results of power for the scenario 1: **a** the wind farm, **b** the 1st WT, **c** the 2nd WT, **d** the 3rd WT

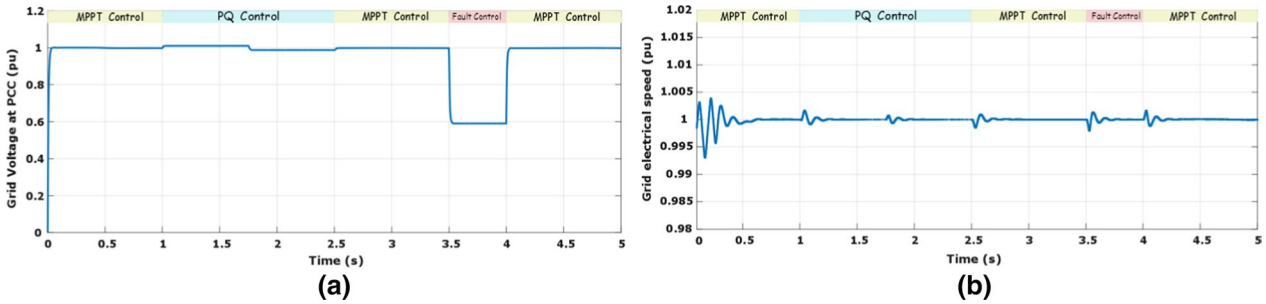

Fig. 14 Simulation results for the scenario-2: **a** grid voltage with 40% dip, **b** electrical angular speed

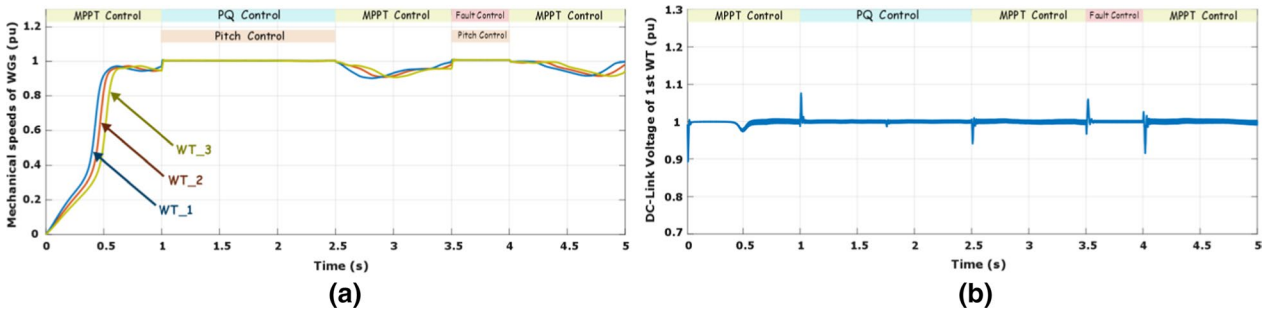

Fig. 15 Simulation results for the scenario-2: **a** mechanical generators speed, **b** DC-link voltage of 1st WT

profiles that are applied to the WTs are shown in Fig. 11.

To verify the effectiveness of the proposed control strategies, the simulation tests are done for both scenarios. They are divided into a number of intervals. In each interval, one of the three operating controls, i.e., MPPT control, PQ control, and voltage fault control, is selected. The voltage fault control mode is activated automatically when one of the measures, such as increase of the current limit or DC-link voltage, appears.

7.1 Scenario 1

The objective of the first scenario is to study and validate the power management and dynamic behavior of the WF and the interaction between WTs, according to a grid operator plan while taking into account the adopted proportional distribution algorithm. The scenario is as follows:

Interval 1: the MPPT control is activated from 0 to 1 s, to provide the maximum active power with unity power factor.
Interval 2: the PQ control is activated from 1 to 2 s. The required active power is equal to 4 MW ($P_{wf}^{ref} = 4\text{MW}$), and for the required reactive power, from 1 to 1.5 s, the WF consumes 2 MVAR while it generates 2 MVAR from 1.5 to 2 s.
Interval 3: the MPPT control is selected from 2 to 3 s.
Interval 4: the PQ control is activated from 3 to 4 s. Similar to interval 2, the required active power is equal to 4 MW, but for reactive power from 3 to 3.5 s, the WF generates 3 MVAR while it consumes maximum reactive power available from 3.5 to 4 s.
Interval 5: the MPPT control is selected from 4 to 5 s.

The simulation results for Scenario 1 are shown in Fig. 12. As shown, the wind farm produces the maximum active power which is the sum of the power of the three WTs, and ensures a unity power factor at PCC during MPPT mode (Fig. 12a). At time t = 1.5 s, a disconnection of the third WT has occurred. This led to the cancellation of its production as shown in Fig. 12d. On the other hand, the power produced by the farm still follows their references, as indicated in Fig. 12a. This is because the other two WTs produce more power to make up for the lost power. Moreover, at 3.5 *s* the transmission system operator demands a maximum reactive power consumption as depicted in Fig. 12. It is distributed in a weighted way over the three WTs (Fig. 12b–d) which shows the

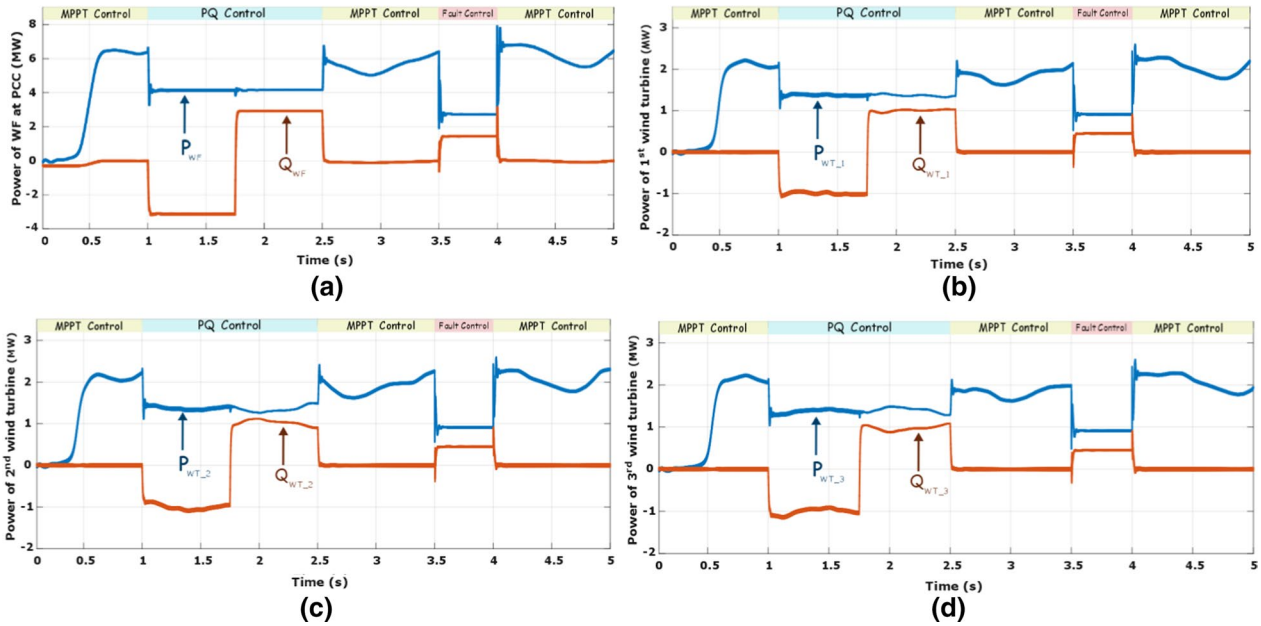

Fig. 16 Simulation results of powers for the scenarion-2: **a** the wind farm, **b** the 1st WT, **c** the 2nd WT, **d** the 3rd WT

application of the proportional distribution algorithm for the centralized supervision of the wind farm power.

7.2 Scenario 2

In the second scenario, in addition to the production of maximum active power and to respect the requested power from the grid operator, this test also uses LVRT in accordance with the German Grid code requirements with an ADRC strategy. This scenario is as follows:

> Interval 1: from 0 to 1 s, the MPPT control is selected to achieve maximum production and ensure a unity power factor at PCC.
> Interval 2: from 1 to 2 s, TSO required active power equal to 4 MW ($P_{wf}^{ref} = 4\text{MW}$), and for the required reactive power from 1 to 1.5 s, the WF consumes 3 MVAR, while from 1.5 to 2 s it generates 3 MVAR reactive power (PQ control).
> Interval 3: from 2.5 to 3.5 s, the MPPT control is selected.
> Interval 4: the fault control is activated from 3.5 to 4 s, with a balanced fault that leads the voltage at PCC to drop to 40% for 500 ms.
> Interval 5: from 4 to 5 s, the MPPT control is selected.

Figure 13 shows the three-phase grid voltage with a symmetrical voltage dip of 40% between 3.5 and 4 s. At the PCC, the grid voltage and the electrical angular speed are shown in Fig. 14.

During the intervals 2 and 4, the generator rotor speeds are increased because of the decreases of the active power transmitted to the network, while through the pitch control, the mechanical speed of the wind generators does not exceed the rated value as illustrated in Fig. 15a. On the other hand, Fig. 15b shows that the DC link voltage of the first WT accurately follows its reference, and after fault occurrence, a limited overvoltage of less than 8% of the rated value is observed, wherein its does not present any threat for the DC bus [23].

Lastly, the simulation results of active and reactive power for scenario 2 are presented in Fig. 16a. With optimal control (MPPT control) the active power produced by the WF at PCC is the sum of the optimal active power of the three WTs and the reactive power at PCC is set to zero. The farm reacts to the active and the reactive power predetermined by the TSO (PQ control) between 1 and 2 s. However, when the grid fault causing a voltage drop of 40% occurred at 3.5 s, it automatically activates the LVRT control. Therefore, in order to regulate the grid voltage in accordance with the German grid code, the WTs inject reactive power (thus reactive current) which is proportional to the gird voltage drop as observed from Fig. 16b–d.

From all the previous simulation results, it can be concluded that the combination of a supervision system based on the proportional distribution algorithm and the ADRC strategy is sufficiently strong and robust, guarantees excellent performances in term of WF active and reactive power management, and enhances voltage stability and security while meeting the grid code requirements.

8 Conclusion

This paper focuses on SCIG-based wind farm management and control strategies, especially the control of active and reactive power at the PCC for a supervisory system based on a proportional distribution algorithm, and considering the FRT capability. The mathematical modeling and design are discussed and a new robust control strategy for the WT is proposed, one which combines Linear Active Disturbance Rejection Control and LVRT control. The three operating modes of WT control are considered. The MPPT control mode is responsible of injecting the maximum power and ensuring a unity power factor at PCC. The PQ control mode is used to provide and consume active and reactive power predetermined by the TSO, while taking into account the limitation of their maximum value. Finally, the fault control mode which is activated automatically when a grid fault occurs using the voltage control method to satisfy the grid code requirements is considered. The results demonstrate that the proposed supervisory control system based on the ADRC strategy has the efficiency to control the active and reactive power of the SCIG-based WF in order to meet the TSO demand and to ride through grid faults while injecting the required reactive power according to German grid code requirements.

Appendix 1

The parameters of the SCIG-based WT system used for the simulation are given in Table 1:

Table 1 Parameters of the SCIG-based WT system

Symbols	Parameters	Values
P_m	Rated mechanical power	2.3339 MW
ω	Rated wind speed	12 m/s
ρ	Density of air	1.225 kg/m^2
R	Blade radius	38.72 m
G	Gearbox ratio	63
P_{wg_n}	Rated active power	2.3 MW
S_{wg_n}	Rated apparent power	2.59 MVA
f_n	Nominal frequency	50 Hz
N_n	Rated rotor speed	1512 tr/min
p	Number of pole pairs	2
R_s	Stator resistance	1.102 Ω
R_r	Rotor resistance	1.497 Ω
$L_{s\sigma}$	Stator leakage inductance	0.06492 mH
$L_{r\sigma}$	Rotor leakage inductance	0.06492 mH
L_m	Magnetizing inductance	2.13461 mH
V_{dc}	DC-link voltage	1320 V
C	DC-link capacitor	17,316.17 μF
R_f	Filter resistance	0.1838 Ω
L_f	Filter inductance	0.61187 mH

Appendix 2

Summary of the supervision algorithm of SCIG-based wind farm for Algorithm 1:

Algorithm 1 Supervision algorithm of wind farm

Estimation: the maximum power of the wind generators $P_{wg\_i}^{max}$ and $Q_{wg\_i}^{max}$.
Estimation: the maximum power of the wind farm P_{wf}^{max} and Q_{wf}^{max}.
Receive: the power references from TSO P_{wf}^{ref} and Q_{wf}^{ref}.
if $P_{wf}^{max} < P_{wf}^{ref}$
  then
  Reduce: the power references of wind farm requested by TSO P_{wf}^{ref} and Q_{wf}^{ref}.
  else
    if Fault=1
      $Q_{wg\_i}^{ref} \longleftarrow Q_{frt\_i}^{ref}$
      $P_{wg\_i}^{ref} \longleftarrow \sqrt{S_{wg\_i}^2 - {Q_{wg\_i}^{ref}}^2}$
    else
      if MPPT=1
        then
          $Q_{wg\_i}^{ref} \longleftarrow 0$
          $P_{wg\_i}^{ref} \longleftarrow P_{opt\_i}$
        else
          if PQ=1
            then
              $Q_{wg\_i}^{ref} \longleftarrow \frac{Q_{wg\_i}^{max}}{Q_{wf}^{max}} Q_{wf}^{ref}$
              $P_{wg\_i}^{ref} \longleftarrow \frac{P_{wg\_i}^{max}}{P_{wf}^{max}} P_{wf}^{ref}$
            End if
          End if
      End if
End if
if $Q_{wg\_i}^{ref} < Q_{wg\_i}^{max}$
  then
    $Q_{wg\_i}^{ref} \longleftarrow Q_{wg\_i}^{ref}$
  else
    $Q_{wg\_i}^{ref} \longleftarrow Q_{wg\_i}^{max}$
End if
if $P_{wg\_i}^{ref} < P_{wg\_i}^{max}$
  then
    $P_{wg\_i}^{ref} \longleftarrow P_{wg\_i}^{ref}$
  else
    $P_{wg\_i}^{ref} \longleftarrow P_{wg\_i}^{max}$
End if

Abbreviations

WF: Wind farm; WG: Wind generator; WT: Wind turbine; SCIG: Squirrel cage induction generator; DFIG: Doubly fed induction generator; PMSG: Permanent magnet synchronous generator; ADRC: Active disturbance rejection control; PI: Proportional integral; TSO: Transmission system operator; CSU:

Central supervision unit; LSU: Local supervision unit; LVRT: Low voltage ride through; FRT: Fault ride through; GC: Grid code; TD: Tracking differentiator; ESO: Extended state observer; NLSEF: Non-linear sate error feedback; LADRC: Linear active disturbance rejection control; PLL: Phase-locked loop; WECS: Wind-Europe's central scenario; MPPT: Maximum power point tracking; PCC: Point of common coupling; PIC: Proportional integral controller; OF: Optimization functions; PD: Proportional distribution; SSC: Stator side converter; GSC: Grid side converter.

Acknowledgements
Not applicable.

Authors' contributions
HL as the corresponding author, proposed the structure and wrote the manuscript, and modelled the system under Matlab Simulink. AE and TN as supervisors contributed to perform and revise the manuscript. All authors read and approve the manuscript.

Funding
The research work is not supported by any funding agency.

Availability of data and materials
Data sharing not applicable to this article as no datasets were generated or analyzed during the current study.

Declarations

Competing interests
The authors declare that they have no known competing financial interests or personal relationships that could have appeared to influence the work reported in this paper.

Author details
[1]Higher National School of Arts and Crafts (ENSAM), Mohammed V University, Rabat, Morocco. [2]National High School for Computer Science and Systems Analysis (ENSIAS), Mohammed V University, Rabat, Morocco.

Received: 6 January 2021 Accepted: 27 January 2022
Published online: 04 March 2022

References

1. Shen, M., Huang, W., Chen, M., et al. (2020). Micro plastic crisis: Unignorable contribution to global greenhouse gas emissions and climate change. *Journal of Cleaner Production, 254*, 120138.
2. Brahimi, T. (2019). Using artificial intelligence to predict wind speed for energy application in Saudi Arabia. *Energies, 12*(24), 4669.
3. Clerk Maxwell, J. (1892). *A treatise on electricity and magnetism,* (Vol. 2, pp. 68–73). Oxford: Clarendon.
4. Diesendorf, M., & Elliston, B. (2018). The feasibility of 100% renewable electricity systems: A response to critics. *Renewable and Sustainable Energy Reviews, 93*, 318–330.
5. Emrad, H. M. (2017). Performance analysis of diode-bridge-type non-superconducting fault current limiter in improving transient stability of DFIG based variable speed wind generator. *Electric Power Systems Research, 143*, 782–793.
6. Pathak, A. K., Sharma, M. P., & Bundele, M. (2015). A critical review of voltage and reactive power management of wind farms. *Renewable and Sustainable Energy Reviews, 51*, 460–471.
7. Chen, Z., Guerrero, J. M., & Blaabjerg, F. (2009). A review of the state of the art of power electronics for wind turbines. *IEEE Transactions on power electronics, 24*(8), 1859–1875.
8. Abhinav, R., & Pindoriya, N. M. (2016). Grid integration of wind turbine and battery energy storage system: Review and key challenges. In *2016 IEEE 6th international conference on power systems (ICPS)* (pp. 1–6), IEEE.
9. Laghridat, H., Essadki, A., Annoukoubi, M., et al. (2020). A novel adaptive active disturbance rejection control strategy to improve the stability and robustness for a wind turbine using a doubly fed induction generator. *Journal of Electrical and Computer Engineering*. https://doi.org/10.1155/2020/9847628
10. Aboudrar, I., El Hani, S., Mediouni, H., et al. (2018). Modeling and robust control of a grid connected direct driven PMSG wind turbine by ADRC. *Advances in Electrical and Electronic Engineering, 16*(4), 402–413.
11. Laghridat, H., Essadki, A., & Nasser, T. (2019). Comparative analysis between PI and linear-ADRC control of a grid connected variable speed wind energy conversion system based on a squirrel cage induction generator. *Mathematical Problems in Engineering*. https://doi.org/10.1155/2019/8527183
12. Tapia, G., Tapia, A., & Ostolaza, J. X. (2006). Two alternative modeling approaches for the evaluation of wind farm active and reactive power performances. *IEEE Transactions on Energy Conversion, 21*(4), 909–920.
13. Fortmann, J., Wilch, M., Koch, F. W., et al. (2008). A novel centralised wind farm controller utilising voltage control capability of wind turbines. In *16th PSCC*, Glasgow, Scotland.
14. Tapia, G., Tapia, A., & Ostolaza, J. X. (2007). Proportional–integral regulator-based approach to wind farm reactive power management for secondary voltage control. *IEEE Transactions on Energy Conversion, 22*(2), 488–498.
15. Rodriguez-Amenedo, J. L., Arnalte, S., & Burgos, J. C. (2002). Automatic generation control of a wind farm with variable speed wind turbines. *IEEE Transactions on Energy Conversion, 17*(2), 279–284.
16. Benlahbib, B., Bouarroudj, N., Bouchafaa, F., et al. (2014). Fractional order PI controller for wind farm supervision. In *2014 IEEE international conference on industrial engineering and engineering management* (pp. 1234–1238), IEEE.
17. Rodriguez-Amenedo, J. L., Arnaltes, S., & Rodriguez, M. A. (2008). Operation and coordinated control of fixed and variable speed wind farms. *Renewable Energy, 33*(3), 406–414.
18. Mahadevan, K., & Kannan, P. S. (2010). Comprehensive learning particle swarm optimization for reactive power dispatch. *Applied Soft Computing, 10*(2), 641–652.
19. Li, Y., Cao, Y., Liu, Z., et al. (2009). Dynamic optimal reactive power dispatch based on parallel particle swarm optimization algorithm. *Computers Mathematics with Applications, 57*(11–12), 1835–1842.
20. Su, X., Mi, Z., Liu, X., et al. Reactive power optimization control of wind farms with fixed-speed wind turbine generators. In *2008 IEEE international conference on sustainable energy technologies* (pp. 972–977), IEEE.
21. Zhao, J., Li, X., Hao, J., et al. (2010). Reactive power control of wind farm made up with doubly fed induction generators in distribution system. *Electric Power Systems Research, 80*(6), 698–706.
22. Ghennam, T., Aliouane, K., Akel, F., et al. (2015). Advanced control system of DFIG based wind generators for reactive power production and integration in a wind farm dispatching. *Energy Conversion and Management, 105*, 240–250.
23. Elyaalaoui, K., Ouassaid, M., & Cherkaoui, M. (2019). Dispatching and control of active and reactive power for a wind Farm considering fault ride-through with a proposed PI reactive power control. *Renewable Energy Focus, 28*, 56–65.
24. An, H., Ko, H., Kim, H., et al. (2012). Modeling and voltage-control of variable-speed SCAG-based wind farm. *Renewable Energy, 42*, 28–35.
25. Huang, Y., & Xue, W. (2014). Active disturbance rejection control: Methodology and theoretical analysis. *ISA Transactions, 53*(4), 963–976.
26. Han, J. (2009). From PID to active disturbance rejection control. *IEEE Transactions on Industrial Electronics, 56*(3), 900–906.
27. Ma, Y., Yang, L., Zhou, X., et al. (2020). Linear active disturbance rejection control for dc bus voltage under low-voltage ride-through at the grid-side of energy storage system. *Energies, 13*(5), 1207.
28. Herbst, G. (2013). A simulative study on active disturbance rejection control (adrc) as a control tool for 658 practitioners. *Electronics, 2*(3), 246–279.
29. Herbst, G. (2015). Practical active disturbance rejection control: Bumpless transfer, rate limitation, and in655 cremental algorithm. *IEEE Transactions on Industrial Electronics, 63*(3), 1754–1762.
30. Ran, M., Wang, Q., Dong, C., et al. (2020). Active disturbance rejection control for uncertain time-delay nonlinear systems. *Automatica, 112*, 108692.
31. Chu, Z. (2018). *Active disturbance rejection control: Applications, stability analysis, and tuning method.*
32. Fu, C., & Tan, W. (2016). Tuning of linear ADRC with known plant information. *ISA Transactions, 65*, 384–393.

33. Gao, R., & Gao, Z. (2016). Pitch control for wind turbine systems using optimization, estimation and compensation. *Renewable Energy, 91*, 501–515.
34. Luo, X., Wang, J., Wojcik, J. D., et al. (2018). Review of voltage and frequency grid code specifications for electrical energy storage applications. *Energies, 11*(5), 1070.
35. Brandao, D. I., Mendes, F. E. G., Ferreira, R. V., et al. (2019). Active and reactive power injection strategies for three-phase four-wire inverters during symmetrical/asymmetrical voltage sags. *IEEE Transactions on Industry Applications, 55*(3), 2347–3235.